Experimental and Computational Study of Solar Air Heater Performance with Ribbed Absorber Plates

Bhushan Meshram[a], Chaitanya Shrivastava[b], Raghvendra Khedle[c]

[a]*Research Scholar , Department Of Mechanical Engineering, Technocrats Institute Of Technology, Bhopal, MP, India*
[b,c] Professor , Department Of Mechanical Engineering, Technocrats Institute Of Technology, Bhopal, MP, India

Abstract. A solar air heater (SAH) is an energy-efficient device designed to harness solar energy to heat air, which can then be used for a wide range of applications such as space heating, industrial processes, ventilation, and drying. Comparison of the experimental and predicted Values of Nusselt Number. It is found that the smooth plate data agree reasonably well with the values predicted. the value of convective heat transfer coefficient increase with the increasing Reynolds Number and increasing the value of roughness. Nusselt number increases with a rise in Reynolds number. The maximum Nusselt number is observed for the 60° double-inclined roughened plate with a 3.5 mm gap. The Nusselt number represents the ratio of conductive resistance to convective resistance in heat flow. As the Reynolds number increases, the boundary layer thickness decreases, leading to a reduction in convective resistance, which subsequently results in a higher Nusselt number. At low Reynolds numbers, the improvement in the Nusselt number compared to a smooth plate is relatively small. This can be attributed to the thicker laminar sublayer, where the flow is slowed down by the roughness elements. Furthermore, the figure demonstrates that the enhancement in heat transfer for roughened plates relative to smooth plates also increases with rising Reynolds numbers.

Keywords: SAH, Nusselt, Air, Temperature, Plate, Reynolds.

1. Introduction
A solar air heater is a device that captures and utilizes solar energy to heat air for various applications. It is a simple, efficient, and environmentally friendly technology that serves as an alternative to conventional heating systems. Solar air heaters are widely used in residential, commercial, and industrial settings to reduce dependency on fossil fuels, lower energy costs, and minimize greenhouse gas emissions.

Fig.1: Solar air heater { https://www.alibaba.com/showroom/heat-pipe-solar-air-heater.html}

1.1. Working Principle

Solar air heaters work by collecting sunlight and converting it into heat. They consist of three main components:

1. Collector Panel: Absorbs solar radiation and converts it into heat. It is typically made of materials like aluminum, copper, or selective coatings that enhance thermal efficiency.

2. Insulation and Enclosure: Prevents heat loss to the surroundings and ensures the efficient transfer of heat to the air.

3. Airflow System: Circulates air through the collector, where it gets heated, and delivers it to the desired location.

Applications

Solar air heaters are versatile and can be used in:

Space Heating: Warming indoor spaces in homes, offices, or greenhouses.

Drying Applications: Drying agricultural products like grains, fruits, and spices.

Industrial Processes: Providing preheated air for industrial drying, curing, and other processes.

2. Experimental Setup

The experimental setup schematic, including the test section, is shown in Figure 2.2. The system consists of:

Entry Section
- Test Section
- Exit Section
- Flow Meter
- Centrifugal Blower

2.1.1 Duct Details

The duct, with internal dimensions of 2043 mm x 200 mm x 25 mm, is constructed from 25 mm thick wooden panels.

• At the exit section, three equally spaced baffles within a 100 mm length ensure uniform temperature mixing (bulk mean temperature).

• The test section measures 1500 mm (33.75 Dh) in length, with entry and exit lengths of 177 mm (2.5√ WH) and 353 mm (5√WH) respectively.

Heating System

• An electric heater (1500 mm x 200 mm) was fabricated using heating wires arranged on a 5 mm asbestos sheet.

• A 1 mm mica sheet between the heater and absorber plate serves as an electrical insulator.

• The back of the heater is insulated with 50 mm glass wool and a 12 mm wooden plate.

Test Surface

• The absorber plate is a 1 mm thick GI sheet with integral rib-roughness, forming the top broad wall of the duct.

• The bottom wall comprises 25 mm wooden panel with insulation beneath.

Insulation and Air Handling

• The duct is insulated with 25 mm polystyrene foam (thermal conductivity: 0.037 W/m•K) along its length.

- Air is circulated using a blower driven by a 3.5 kW, 440 V, three-phase AC motor, with flow controlled by   a gate valve.

2.2.2 Instrumentation

1. Temperature Measurement:

Calibrated copper-constantan thermocouples (0.3 mm) are placed along the axial centerline of the absorber   plate at equal intervals of 21.4 cm.

Bulk air inlet and outlet temperatures are measured with a standard mercury thermometer (least count: 0.1°C).

A digital micro voltmeter records thermocouple readings, and calibration ensures ±1°C accuracy.

2. Airflow Measurement:

A pre-calibrated orifice meter is installed in a 53 mm diameter pipe to measure airflow rates.

An inclined tube manometer (least count: 0.1 cm Hg) measures pressure drop across the orifice plate.

3. Pressure Drop Measurement:

A micro-manometer (least count: 0.0025 mm) measures pressure drops across the duct and test section.

The manometer includes a movable reservoir to minimize capillary and meniscus errors.

3. Experimental Procedure

3.1.1 Setup Checks:

All instruments and components are inspected for proper operation.

Air leakage is checked using the soap bubble technique.

3.1.2   Temperature Stabilization:

The test setup is pre-heated to achieve steady-state conditions (constant temperature at any point for 10-12 minutes).

Changes in operating conditions require 30-40 minutes to re-stabilize.

3.1.3   Data Collection:

Temperature readings are recorded using thermocouples and a digital voltmeter.

Pressure drops across the orifice plate and duct are measured using manometers.

For each rib configuration, five test runs are conducted at Reynolds numbers ranging from 4000 to 14,000.

3.1.4   Steady-State Conditions:

Steady-state is confirmed when outlet and plate temperatures remain constant over 15 minutes.

Tests are conducted with a temperature difference of at least 20°C between the heated plate and bulk air   temperature.

Recorded Parameters

1. Pressure drop across the orifice plate.
2. Pressure drop within the duct.
3. Inlet and outlet air temperatures.
4. Plate temperature.

Fig. 2: Photograph of experimental set up & Actual Test Section.

3.2   Thermo hydraulic performance

The heat transfer and friction characteristics of a roughened duct indicate that an improvement in heat transfer is typically accompanied by a penalty in friction power due to an increase in the friction factor. Consequently, it becomes crucial to identify a geometric configuration that maximizes heat transfer enhancement while minimizing the friction-related penalty.

To address this dual objective of optimizing both thermal and hydraulic performance—referred to as thermo-hydraulic performance—Lewis [15] introduced a parameter known as the **efficiency parameter (η).** This parameter evaluates the enhancement in heat transfer achieved in a roughened duct relative to a smooth duct under the condition of equal pumping power requirements. The efficiency parameter (η) provides a quantitative measure for comparing and optimizing the performance of duct geometries.

$$T_{hp} = (Nu \ / \ Nus) \ / \ (fr \ / \ fs)^{1/3}$$

A value of the efficiency parameter greater than unity indicates the effectiveness of using an enhancement device and serves as a basis for comparing the performance of various configurations to determine the optimal arrangement. The performance of different roughness geometries is analyzed using this parameter.

Thermo-hydraulic performance is evaluated using the following calculation:

$$T_{hp} = (N_u \ / N_{us}) \ / \ (f_r \ / \ f_s)^{1/3}$$

4. Result and Discussion

Fig. 3 shows the comparison of the experimental and predicted Values of Nusselt Number. It is found that the smooth plate data agree reasonably well with the values predicted.

$$Nus = 0.024 Re^{0.8} Pr^{0.4} \ldots \ldots \ldots (4.1)$$

It is also seen from the fig. (3.1) that Nusselt Number increase with Reynolds Number.
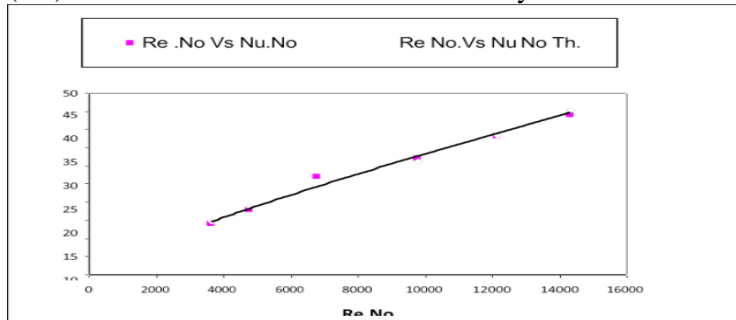
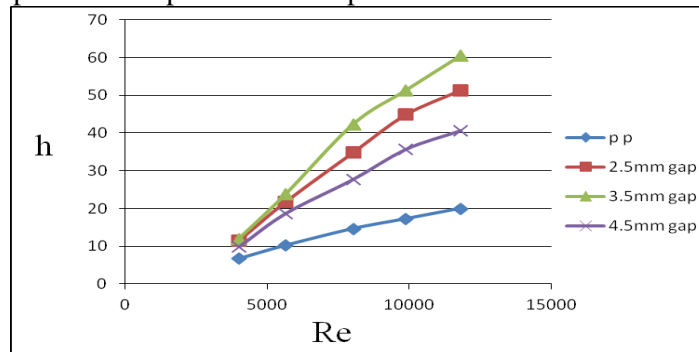Fig .3: Comparison of experimental and predicted value of Nusselt No.

Fig. 4: Comparison of experimental data of rough plate with sooth plate.
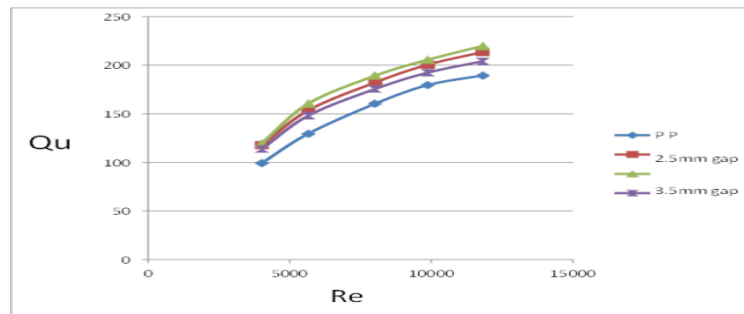

Fig. 5: comparison of heat gained by air Vs Reynolds no.

It can be seen from the fig. 5 shows the value of convective heat transfer coefficient increase with the increasing Reynolds Number and increasing the value of roughness.
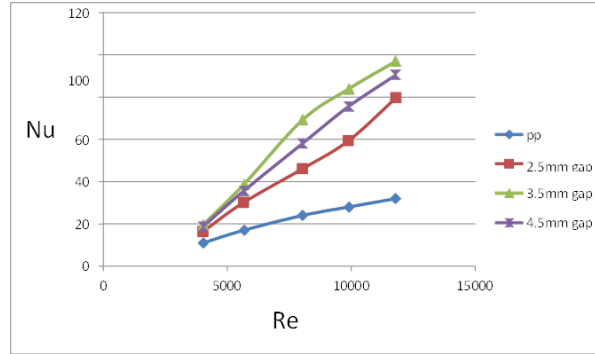
Fig. 6: Nusselt Number Vs Reynolds Number.

As illustrated in Fig.6, the Nusselt number increases with a rise in Reynolds number. The maximum Nusselt number is observed for the 60° double-inclined roughened plate with a 3.5 mm gap. The Nusselt number represents the ratio of conductive resistance to convective resistance in heat flow. As the Reynolds number increases, the boundary layer thickness decreases, leading to a reduction in convective resistance, which subsequently results in a higher Nusselt number.

At low Reynolds numbers, the improvement in the Nusselt number compared to a smooth plate is relatively small. This can be attributed to the thicker laminar sublayer, where the flow is slowed down by the roughness elements. Furthermore, the figure demonstrates that the enhancement in heat transfer for roughened plates relative to smooth plates also increases with rising Reynolds numbers.
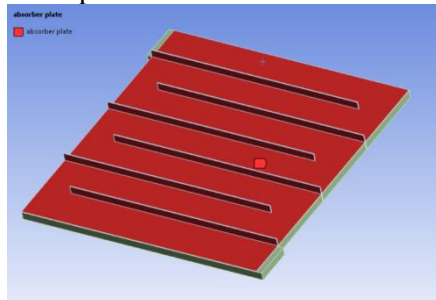

Fig.7: Absorber plate, which made of aluminium and copper.

Case design

One case is investigating in this study as mention in table .1 As mention in table 1 material use for absorber plate with 2 different mass flow inlet of air.

Table.1 Case Description

Cases	Absorber plate material	Mass flow inlet (kg/s)
Case - 1	Aluminum	0.00321

5. Results

The numerical design and evaluation is focussed on the measurement of main parameters of the SAH, namely the temperature distributions in the SAH, the ambient conditions, mass flow rates and absorber plate material. Furthermore, a flowchart of the CFD procedure is given Figure 8

The temperature distribution in the working fluid is presented for a surface in the middle of the front and rear cavity which is formed between glass and absorber plate in both side. Similar temperature contour are observed in both the front and rear channels for remaining cases. The colour gradient represent the temperature value of the working fluid in Kelvin (K). Blue and red colour represent the minimum and maximum value of the temperature.
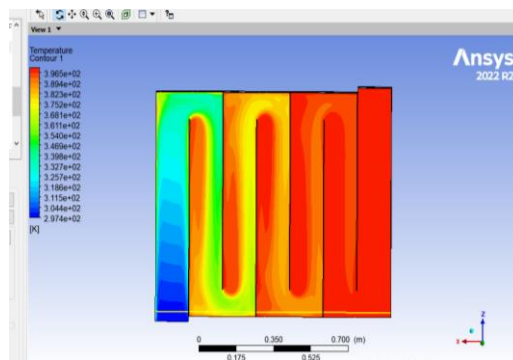

Fig. 8: Temperature at plane above absorber plate in with 3.5 mm gap.

Temperature contour

Heat transfer between the absorber surface and the working fluid is influenced by the fluid's mass flow rate. In this case, air flows through the cavity at a mass flow rate of 0.00321 kg/s, with the absorber made of aluminum. At higher mass flow rates, the heat transfer becomes less effective due to the reduced contact time between the air and the absorber surface.

Figures 8 illustrate the temperature distribution in the fluid above and below the absorber plate. The color gradient represents specific temperature values within different regions of the air heater. At the inlet, the air temperature is shown in blue, corresponding to 297 K. As the simulation progresses, the air flows through the heater and reaches different zones where the fluid color transitions to green, indicating a temperature range of 340 K to 360 K.

Further along the heater, the color changes to brown, representing fluid temperatures ranging from 380 K to 396.5 K. Due to the high mass flow rate, the air achieves a temperature of 396.5 K approximately halfway along the total distance from the inlet to the outlet.

6. Conclusion

This study presents an extensive investigation of 60° double-inclined ribs with a gap as artificial roughness on the underside of one broad wall of a solar air heater. The results were compared with those of a smooth duct under similar flow conditions to examine variations in the Nusselt number.

The following conclusions were drawn from the research:

1.Throughout the entire range of Reynolds numbers, the Nusselt number was found to increase, peaking for a roughened plate with 60° double-inclined ribs and a 3.5 mm gap. Further improvements in the roughness geometry led to additional increases in the Nusselt number.

2. The thermo-hydraulic performance of three roughened absorber plates was experimentally evaluated and compared with that of a smooth plate. The 60° double-inclined ribbed plate with a 3.5 mm gap demonstrated the best thermo-hydraulic performance. However, it was noted that further increasing the roughness beyond a 3.5 mm gap yielded only marginal improvements in thermo-hydraulic performance.

Acknowledgements

References

[1] kumar, R., Kumar, R., Kumar, S., Thapa, S., Sethi, M., Fekete, G., & Singh, T. , Impact of artificial broughness variation on heat transfer and friction characteristics of solar air heating system. Alexandria Engineering Journal, 61(1), 481–491, 2022, https://doi.org/10.1016/j.aej.2021.06.031.

[2] Hassan, H., S. Yousef, M., & Abo-Elfadl, S. Energy, exergy, economic and environmental assessment of double pass V-corrugated-perforated finned solar air heater at different air mass ratios. Sustainable Energy Technologies and Assessments, 43(December 2020), 100936. https://doi.org/10.1016/j.seta.2020.100936.

[3] Ganesh Kumar, P., Balaji, K., Sakthivadivel, D., Vigneswaran, V. S., Velraj, R., & Kim, S. C, Enhancement of heat transfer in a combined solar air heating and water heater system. Energy, 221, 119805. https://doi.org/10.1016/j.energy.2021.119805

[4] Kumar, P. G., Sakthivadivel, D., Balaji, K., Salman, M., & Kim, S. C. Performance enhancement of a double-pass solar air heater with a shot-blasted absorber plate and winglets. Journal of Mechanical Science and Technology, 35(6), 2743–2753.2021, https://doi.org/10.1007/s12206-021-0544-x

[5] Baissi, M. T., Brima, A., Aoues, K., Khanniche, R., & Moummi, N. Thermal behavior in a solar air heater channel roughened with delta-shaped vortex generators. Applied Thermal Engineering, 165(August 2020), 113563. https://doi.org/10.1016/j.applthermaleng.2019.03.13

[6] Khanlari, A., Güler, H. Ö., Tuncer, A. D., Şirin, C., Bilge, Y. C., Yılmaz, Y., & Güngör, A. ,Experimental and numerical study of the effect of integrating plus-shaped perforated baffles to solar air collector in drying application. Renewable Energy, 145, 1677–1692, 2020https://doi.org/10.1016/j.renene.2019.07.076

[7] Khanlari, A., Sözen, A., Afshari, F., Şirin, C., Tuncer, A. D., & Gungor, A. Drying municipal sewage sludge with v-groove triple-pass and quadruple-pass solar air heaters along with testing of a solar absorber drying chamber. Science of the Total Environment, 709. 2020, https://doi.org/10.1016/j.scitotenv.2019.136198

[8] Saravanakumar, P. T., Somasundaram, D., & Matheswaran, M. M., Exergetic investigation andn optimization of arc shaped rib roughened solar air heater integrated with fins and baffles. Applied ThermalEngineering,175(November2020),115316. https://doi.org/10.1016/j.applthermaleng.2020.115316

[9] Tou ili, S., Alami Merrouni, A., El Hassouani, Y., Amrani, A. illah, & Rachidi, S. Analysis of the yield and production cost of large-scale electrolytic hydrogen from different solar technologies and under several Moroccan climate zones. International Journal of Hydrogen Energy, 45(51), 26785–26799.2020, https://doi.org/10.1016/j.ijhydene.2020.07.118

[10] Kumar, A., & Layek, A. Energetic and exergetic performance evaluation of solar air heater with twisted rib roughness on absorber plate. Journal of Cleaner Production, 232, 617–628.2019 https://doi.org/10.1016/j.jclepro.2019.05.363.

[11] Hu, J., Liu, K., Guo, M., Zhang, G., Chu, Z., & Wang, M. Performance improvement of baffle- type solar air collector based on first chamber narrowing. Renewable Energy, 135, 701–710, 2019 https://doi.org/10.1016/j.renene.2018.12.049.

[12] Abuşka, M. Energy and exergy analysis of solar air heater having new design absorber plate with conical surface. Applied Thermal Engineering, 131, 115–124.2018,https://doi.org/10.1016/j.applthermaleng.2017.11.129.

[13] Allouhi, A., Benzakour Amine, M., Saidur, R., Kousksou, T., & Jamil, A. Energy and exergy analyses of a parabolic trough collector operated with nanofluids for medium and high temperature applications. Energy Conversion and Management, 155(October 2017), 201–217. https://doi.org/10.1016/j.enconman.2017.10.05.

[14] Ghiami, A., & Ghiami, S. (2018). Comparative study based on energy and exergy analyses of a baffled solar air heater with latent storage collector. Applied Thermal Engineering, 133, 797–808.2018, https://doi.org/10.1016/j.applthermaleng.2017.11.111.

[15] Hassan, H., & Abo-Elfadl, S. Experimental study on the performance of double pass and two inlet ports solar air heater (SAH) at different configurations of the absorber plate. Renewable Energy, 116, 728–740.2017 https://doi.org/10.1016/j.renene.